Functional homo- and heterodimeric actin capping proteins from the malaria parasite

Ábris Ádám Bendes[a], Moon Chatterjee[b], Benjamin Götte[b], Petri Kursula[a,c], Inari Kursula[a,b,c*]

[a]Biocenter Oulu and Faculty of Biochemistry and Molecular Medicine, University of Oulu, P.O. Box 5400, 90014 Oulu, Finland

[b]Centre for Structural Systems Biology – Helmholtz Centre for Infection Research and DESY, Notkestrasse 85, 22607 Hamburg, Germany

[c]Department of Biomedicine, University of Bergen, Jonas Lies vei 91, 5009 Bergen, Norway

[*]Corresponding author: inari.kursula@uib.no, +47 55586846

Other authors' e-mail addresses: abris.bendes@oulu.fi, moon.chatterjee@yale.edu, benjamin.gotte@ki.se, petri.kursula@uib.no

Running title: *Plasmodium* actin capping proteins

ABSTRACT

Actin capping proteins belong to the core set of proteins minimally required for actin-based motility and are present in virtually all eukaryotic cells. They bind to the fast-growing barbed end of an actin filament, preventing addition and loss of monomers, thus restricting growth to the slow-growing pointed end. Actin capping proteins are usually heterodimers of two subunits. The *Plasmodium* orthologs are an exception, as their α subunits are able to form homodimers. We show here that, while the β subunit alone is unstable, the α subunit of the *Plasmodium* actin capping protein forms functional homo- and heterodimers. This implies independent functions for the αα homo- and αβ heterodimers in certain stages of the parasite life cycle. Structurally, the homodimers resemble canonical αβ heterodimers, although certain rearrangements at the interface must be required. Both homo- and heterodimers bind to actin filaments in a roughly equimolar ratio, indicating they may also bind other sites than barbed ends.

Keywords: actin; capping protein; heterodimer; homodimer; *Plasmodium*; malaria

Abbreviations: CP – actin capping protein; CapZαβ – *Gallus gallus* CP; F – filamentous; G – globular; *Pb – Plasmodium berghei*; *Pf – Plasmodium falciparum*; ActI – actin isoform I;

INTRODUCTION

Actin, a central component of the cytoskeleton, is essential for a plethora of cellular functions, including cell motility from amoeboid crawling that exploits extensive filamentous (F-)actin networks at the leading edge to the mechanistically similar intracellular dashing of pathogenic bacteria using comet tails built up of host actin [1]. The ability to form dynamic, long filaments with a defined polarity enables actin to fulfill its versatile functions. Filament dynamics in opisthokonts are regulated by >100 accessory proteins [2]. Actin capping proteins (CPs) belong to the core set of proteins needed to reconstitute actin-based motility *in vitro* [3]. CPs are found in essentially all eukaryotic organisms and cell types [4–6] and bind to F-actin barbed ends, blocking subunit exchange at the fast-growing end and limiting growth to the pointed end [6–8]. In addition, they display nucleation activity [7].

In almost all organisms investigated to date, CPs are heterodimers of two subunits [6,9]. An exception is the malaria parasite (*Plasmodium berghei*), which belongs to the phylum *Apicomplexa* [10,11]. Apicomplexan gliding is a special form of actin-based motility, and its molecular mechanisms are poorly understood. Unlike the slow amoeboid crawling, gliding is fast (1-3 μm/s) and does not involve notable changes in cell shape [12–14]. Most apicomplexan actins do not readily form long filaments, and their polymerization kinetics differ from canonical actins [15–21]. The lack of fine-tuning of polymerization is underlined by the minimal set of actin regulatory proteins present in *Apicomplexa* [22,23].

Apicomplexa also have two CP subunits. The *P. berghei* CP β subunit (*Pb*CPβ) is essential for sporozoite motility in the mosquito vector [10]. However, its deletion does not influence blood-stage development in the mammalian host. Unlike *Pb*CPβ, the gene encoding the *P. berghei* CP α subunit (*Pb*CPα) is not upregulated upon sporozoite maturation [24]. Earlier, it was shown that *Pb*CPα can form homodimers, which bind to vertebrate skeletal muscle α-actin [11]. Here, we set out to characterize the *Pb*CPαα homodimers as well as *Pb*CPαβ heterodimers. We show that both bind to parasite actin filaments and share a highly similar secondary and quaternary structure.

MATERIALS AND METHODS

Protein expression and purification

A construct encoding *Pb*CPα (*Pb*CPαα; PlasmoDB: PBANKA_1243100) was subcloned into the pETM-14 vector to introduce a 3C protease-cleavable N-terminal His$_6$-tag. Amino acids 1-287 were subcloned into a pNIC-Bsa4 derivative vector to create the construct *Pb*CPαα$^{\Delta C20}$ with a C-terminal His$_6$-tag substituting the last 20 residues (so-called α-tentacle). A *Pb*CPαβ construct was prepared by subcloning untagged *Pb*CPα together with a C-terminally His$_6$-tagged *Pb*CPβ (PlasmoDB: PBANKA_1232400) into the pFastBac Dual vector. *Pb*CPαα was expressed in *Escherichia coli* BL21(DE3) RARE, while *Pb*CPαα$^{\Delta C20}$ and *Gallus gallus* CP (CapZαβ) [9] were expressed in *E. coli* BL21(DE3) RIPL, each for 16 h at 15°C after IPTG induction in LB medium. *Pb*CPαβ was expressed using *Spodoptera frugiperda Sf*21 cells for 4 days after infection in Insect-XPRESS medium (Lonza, CH), as the heterodimer could not be expressed in soluble form in bacteria. We were unable to express the *Pb*CPβ alone.

All purification steps were performed on ice or at 4°C, unless otherwise stated. *Pb*CPαα and *Pb*CPαβ were lysed using freeze-thaw cycles in a lysis buffer containing 50 mM HEPES (pH 8.0), 400 mM NaCl, 7.5 mM imidazole, 5 mM β-ME, and 1X protease inhibitor cocktail (S8830, Sigma-Aldrich, US). All buffers for *Pb*CPαα prior to size-exclusion chromatography (SEC) were supplemented with 0.5 mM PMSF, while 5% glycerol, 50 mM arginine, and 50 mM glutamate were added to the *Pb*CPαβ buffers. Lysates were cleared by centrifugation (45000 *g*, 30 min) and loaded on HisPur Ni-NTA resin (Thermo Scientific, US). The matrix was washed with a buffer containing 50 mM HEPES (pH 8.0), 100 mM NaCl, 30 mM imidazole, and 5 mM β-ME. The proteins were eluted with 50 mM HEPES (pH 8.0), 50 mM NaCl, 250 mM imidazole, and 5 mM β-ME. The His$_6$-tag of *Pb*CPαα was cleaved off by 3C protease digestion for 30 min and subsequently loaded on Q Sepharose FF resin (GE Healthcare, US). The flow-through fractions were collected and combined with fractions from a subsequent imidazole-free wash. *Pb*CPαα$^{\Delta C20}$ and CapZαβ were lysed using sonication in a lysis buffer containing 50 mM HEPES (pH 8.0), 100 mM NaCl, 5 mM imidazole, and 5 mM β-ME or 20 mM TRIS-HCl (pH 8.0), 100 mM NaCl, and 5 mM β-ME,

respectively. 1X protease inhibitor cocktail was added to the lysis buffers. Lysates were cleared by centrifugation (45000 g, 30 min) and loaded on HisPur Ni-NTA resin. The matrix was washed with the lysis buffer complemented by 1 M NaCl and 20 mM imidazole followed by 50 and 30 mM imidazole for PbCPαα$^{\Delta C20}$ and CapZαβ, respectively. After elution with 300 mM imidazole in the lysis buffer, the fractions were exchanged through a PD10 column (GE Healthcare, US) to 20 mM HEPES (pH 8.0), 20 mM NaCl, and 5 mM β-ME or 20 mM TRIS-HCl (pH 8.0), 50 mM NaCl, and 5 mM β-ME for PbCPαα$^{\Delta C20}$ and CapZαβ, respectively. The proteins were loaded, respectively, on SP and Q Sepharose FF resins (GE Healthcare, US), washed, and eluted using 300 mM NaCl supplemented wash buffers. Fractions containing CPs were concentrated and finally purified using SEC on a Superdex 200 Increase 10/300 column (GE Healthcare, US) using a buffer containing 50 mM HEPES (pH 8.0), 100 mM NaCl, and 0.5 mM TCEP (SEC buffer). The purity of the CPs was confirmed using SDS-PAGE. *Plasmodium falciparum* actin isoform I (*Pf*ActI) was expressed and purified as previously described [18,25].

Molecular mass determination

For molecular mass determination, 25 μl *Pb*CPαα (4.5 mg/ml) or *Pb*CPαα$^{\Delta C20}$ (2.2 mg/ml) were applied to a Superdex 200 Increase 10/300 column, equilibrated with 50 mM HEPES (pH 8.5), 450 mM NaCl, and 0.5 mM TCEP, at a flow rate of 0.5 ml/min. The system was attached to a miniDAWN TREOS multi-angle static light scattering (SLS) detector (Wyatt Technology, US) and a RI-101 differential refractometer (Shodex, US). Bovine serum albumin (Sigma-Aldrich, US) was used for calibration. Molecular weights were determined based on the measured SLS and refractive index or UV signal using the ASTRA software (Wyatt Technology, US).

Folding analysis

The CPs were dialyzed to a buffer containing 10 mM Na-phosphate (pH 8.0) and 100 mM NaF and diluted to 0.25-0.45 mg/ml. Circular dichroism (CD) spectra using synchrotron

radiation (SR) were measured on the AU-CD beamline at the ASTRID2 synchrotron (ISA, Aarhus, Denmark). CD spectra between 170 and 280 nm were recorded in a 0.1-mm quartz cuvette at 10°C. Smoothed SRCD spectra were deconvolved into secondary structure components with the BeStSel [26] server using data between 175 and 250 nm.

Thermal unfolding assays

The CPs were diluted in SEC buffer to 0.3 mg/ml with 1X SYPRO Orange dye (Invitrogen, US). Heat denaturation was followed in triplicates on an Applied Biosystems 7500 real-time PCR system (Thermo Scientific, US) over a range of 25-89°C in 1°C/min steps. Melting temperatures (T_m) were calculated from a Boltzmann fit to the raw data.

Small-angle X-ray scattering and molecular modeling

Small-angle X-ray scattering (SAXS) coupled with SEC was measured on the Diamond Light Source B21 beamline (Didcot, UK) with a Pilatus 2M detector spanning a scattering vector range of 0.0032 to 0.38 Å^{-1}. 45 µl of PbCPαα$^{\Delta C20}$ at 10 mg/ml were applied onto a Superdex 200 Increase 3.2/300 column (GE Healthcare, US) at 22°C with a 0.075 ml/min flow rate using the SEC buffer used in purification, supplemented with 3% (v/v) glycerol. Data reduction and analysis were carried out with ScÅtter [27] and the ATSAS [28] package. *Ab initio* bead models were built using DAMMIN [29] from 23 averaged DAMMIF [30] models. For further analysis, a model of PbCPαα$^{\Delta C20}$ was prepared using a SWISS-MODEL [31] generated PbCPαβ model as a scaffold and exchanging each subunit with a truncated PbCPα$^{\Delta C20}$ monomer. The assembled model was subsequently aligned with the DAMMIN envelope using SASPY plugin [32] of PyMOL [33] and manually adjusted.

Actin cosedimentation assays

The cosedimentation assays were performed as previously described [34] with minor modifications. The CPs were diluted in F-buffer [50 mM KCl, 4 mM MgCl$_2$, 1 mM EGTA

(pH 8.0)] and incubated with F-*Pf*ActI for either 15 min or 8-16 h (ON) at 22°C where relevant, prior to ultracentrifugation. Globular (G-)*Pf*ActI samples were prepared in G-buffer [10 mM HEPES (pH 7.5), 0.2 mM $CaCl_2$, 0.5 mM TCEP, 0.5 mM ATP].

RESULTS AND DISCUSSION

Plasmodium actin capping proteins form folded homo- and heterodimers in solution

*Pb*CPβ is dispensable for parasite survival in the mammalian host [10], indicating that the α subunit may function as a separate unit. Independent functions of CP subunits have not been described in any other eukaryote; recombinant expression of individual subunits typically produces insoluble protein [35], and active recombinant CP is only achieved by coexpression of both subunits [36]. Conversely, *Pb*CPα can be expressed alone in soluble form [11]. We expressed recombinantly the *Pb*CPαβ heterodimer, as well as two versions of the *Pb*CPαα homodimer; the full-length protein and a version lacking the C-terminal tentacle. Size exclusion chromatography combined with SLS indicated molecular weights of 66.44±0.13 kDa for *Pb*CPαα and 63.55±0.13 kDa for *Pb*CPαα$^{\Delta C20}$ **(Fig 1A)**. These are very close to the expected molecular weights of the full-length (72 kDa) or truncated (68 kDa) homodimer. CD spectroscopy showed that all three parasite CPs have a folded structure with secondary structure contents roughly similar to the CapZαβ heterodimer **(Fig 1B)**. The parasite CPs were profoundly less thermostable than CapZαβ with melting temperatures around 46-49°C compared to 58°C of CapZαβ **(Fig 2 and Suppl. Fig 1)**. The high initial fluorescence **(Fig 2B)** and negative unfolding signal **(Suppl. Fig 1B)** may indicate a less compact structure with more solvent-exposed hydrophobic surface in the homodimers compared to the heterodimers. The full-length homodimer was the least stable of all CPs.

We determined the solution structure of *Pb*CPαα$^{\Delta C20}$ using SAXS **(Fig 3)**. *Ab initio* model building suggests a folded molecule with 2-fold symmetry and a mushroom-like shape **(Fig 3)**, which resembles the CapZαβ heterodimer. A homology model of the *Pb*CPαα$^{\Delta C20}$ homodimer based on the crystal structure of CapZαβ [9] fits well into the SAXS envelope **(Fig 3C)** and reasonably to the raw scattering data **(Suppl. Fig. 2)**. The fits indicate that the

homodimer in solution is somewhat longer and possibly more flexible than the homology model suggests. Based on the homology model, a *Pb*CPαα dimer would also be preferred over a monomer, as taking the subunits out of their dimer context would expose a large hydrophobic interface.

For the barbed-end capping activity, the C-terminal tentacles of each CP subunit are crucial. In CapZαβ, deletion of the α-tentacle is more detrimental for the overall function than the loss of the β-tentacle [37]. Basic residues of the α-tentacle initially interact with acidic amino acids of the penultimate and last actin protomers [38]. The mobile β-tentacle then occupies a hydrophobic pocket on the terminal protomer [38]. The residues Lys278, Lys282, and Lys290 in the α-tentacle, important for actin binding in CapZαβ [38,39], are conserved in *Pb*CPα.

*Pb*CPα contains a *Plasmodium*-specific 23-residue insertion between α-helix 4 and β-strand 7 [11], which our models suggest to lie close to the C terminus and the expected actin-binding surface. Thus the orientation of the α-tentacles in the *Pb*CPαα homodimer might not be identical to the CapZαβ heterodimer. Also, α-helix 4 and β-strand 7 may have to move to accommodate this extension in the homodimer. In agreement with the thermal denaturation data, these structural rearrangements compared to CapZαβ are likely to lead to different dimerization and actin-binding interfaces, and the role of the C terminus of the parasite protein may not be conserved. Earlier, we have described a similar parasite-specific insertion implicated in actin binding in *P. falciparum* profilin [40,41].

CPs are expressed throughout the *Plasmodium* life cycle [10], but the two subunits apparently have partly independent roles. Possibly, CPβ mediates microfilament capping in the mosquito stages, whereas CPα may have evolved for functions in the warm-blooded mammalian host. Notably, *Plasmodium* also has two actin isoforms, of which actin II has specific functions during the sexual reproduction in the mosquito [17,42], whereas actin I is expressed in all stages and required for motility [12,43]. The two actin isoforms have different filament lengths and structures [17] and thus may need CPs with different binding properties. It remains to be investigated, whether the different CP dimers have different specificities towards the two actin isoforms. Higher animals express several isoforms of both

CPα and CPβ with tissue-specific expression patterns [44–46]. Similarly, *Pb*CPβ was initially identified as a gene up-regulated during sporozoite maturation [24]. While the two CP subunits seem to have separate roles in *Plasmodium*, differential and tissue-specific heterodimers are established in other organisms. For instance, in mouse muscle cells, the two CPβ isoforms perform distinct functions that cannot be complemented by the other isoform [46].

Plasmodium CPαα homodimers as well as CPαβ heterodimers bind to parasite actin filaments

The C terminus of CapZβ in the heterodimer is important for stabilizing the capping complex at the barbed end, while CapZα is mainly responsible for initial recognition and binding to the filament [37–39]. The *Pb*CPαα homodimer binds to vertebrate skeletal muscle actin filaments [11], but so far, no studies have been undertaken using parasite actins. Therefore, we set out to test whether the *Pb*CPαα homodimer interacts with *Pf*ActI filaments. Surprisingly, CapZαβ did not significantly cosediment with *Pf*ActI **(Fig 4A)**, whereas *Pb*CPαβ and both the full-length and truncated *Pb*CPαα homodimers were present in the pellet fractions in an apparently equimolar ratio to actin, confirming their binding to parasite F-actin and suggesting they may bind also to the sides of filaments **(Fig 4B-D)**. Another possible reason for the high binding ratio would be the short length of the *Pf*ActI filaments [17]. In particular the full-length homodimer increased the amount of actin in the soluble fraction, indicating that it either sequesters monomers or short oligomers, or shortens the filament length such that they do not pellet anymore. The same was true also for CapZαβ, despite it not stably binding to the filaments **(Fig 4A)**. The fact that *Pb*CPαα$^{\Delta C20}$ cosediments with parasite actin filaments suggests that the role of the α-tentacle may be less pronounced in the initial recognition and stable binding of the homodimers to *Pf*ActI filaments.

Interestingly, the full-length homodimer shows a substantial amount of degradation (labeled as 'fragment' in **Fig 4C**). We have not been able to eliminate this degradation using

protease inhibitors or mutagenesis, and the apparently same degradation product was present also in an earlier study [10]. The degradation seems to plateau at an approximate 1:1 ratio of full-length and degraded PbCPαα **(Suppl. Fig 3A),** and the cleaved product corresponds roughly to our truncated PbCPαα$^{\Delta C20}$ **(Suppl. Fig 3B)**. This poses the question, whether the degradation of the C-terminal tentacle might be biologically relevant and required for the correct formation of the homodimer. This is supported by the higher T_m of PbCPαα$^{\Delta C20}$ compared to the full-length homodimer.

Concluding remarks

The CPα subunit of the malaria parasite is the first example of a CP able to form stable, functional homodimers in solution, indicating that it may have cellular functions independent of the β subunit. Although exclusively dimeric *in vitro*, we cannot exclude that PbCPα could exist as a mixture of monomers and dimers *in vivo*, and α/β heterodimers very likely also have a significant role during the parasite life cycle. These remain important topics for biochemical, structural, and *in vivo* studies and may open possibilities for malaria intervention strategies. Our findings warrant future work addressing whether CP homodimers could exist and perform certain roles in other eukaryotes.

CONFLICT OF INTEREST

The authors declare that they have no conflict of interest.

REFERENCES

[1]   L.A. Cameron, P.A. Giardini, F.S. Soo, J.A. Theriot, Secrets of actin-based motility revealed by a bacterial pathogen, Nat. Rev. Mol. Cell Biol. 1 (2000) 110–119. https://doi.org/10.1038/35040061.

[2]   T.D. Pollard, J.A. Cooper, Actin, a central player in cell shape and movement, Science (80-.). 326 (2009) 1208–1212. https://doi.org/10.1126/science.1175862.

[3]   T.P. Loisel, R. Boujemaa, D. Pantaloni, M.F. Cartier, Reconstitution of actin-based motility of Listeria and Shigella using pure proteins, Nature. 401 (1999) 613–616. https://doi.org/10.1038/44183.

[4]   J. Xu, J.F. Casella, T.D. Pollard, Effect of capping protein, CapZ, on the length of actin filaments and mechanical properties of actin filament networks, Cell Motil. Cytoskeleton. 42 (1999) 73–81. https://doi.org/10.1002/(SICI)1097-0169(1999)42:1<73::AID-CM7>3.0.CO;2-Z.

[5]   J.A. Cooper, D. Sept, New Insights into Mechanism and Regulation of Actin Capping Protein, Int. Rev. Cell Mol. Biol. 267 (2008) 183–206. https://doi.org/10.1016/S1937-6448(08)00604-7.

[6]   M.A. Wear, J.A. Cooper, Capping protein: New insights into mechanism and regulation, Trends Biochem. Sci. 29 (2004) 418–428. https://doi.org/10.1016/j.tibs.2004.06.003.

[7]   J.E. Caldwell, S.G. Heiss, V. Mermall, J.A. Cooper, Effects of CapZ, an Actin Capping Protein of Muscle, on the Polymerization of Actin, Biochemistry. 28 (1989) 8506–8514. https://doi.org/10.1021/bi00447a036.

[8]   J.A. Cooper, T.D. Pollard, Effect of Capping Protein on the Kinetics of Actin Polymerization, Biochemistry. 24 (1985) 793–799. https://doi.org/10.1021/bi00324a039.

[9]   A. Yamashita, K. Maeda, Y. Maéda, Crystal structure of CapZ: Structural basis for actin filament barbed end capping, EMBO J. 22 (2003) 1529–1538. https://doi.org/10.1093/emboj/cdg167.

[10]   M. Ganter, H. Schüler, K. Matuschewski, Vital role for the Plasmodium actin capping protein (CP) beta-subunit in motility of malaria sporozoites, Mol. Microbiol. 74 (2009) 1356–1367. https://doi.org/10.1111/j.1365-2958.2009.06828.x.

[11]   M. Ganter, Z. Rizopoulos, H. Schüler, K. Matuschewski, Pivotal and distinct role for Plasmodium actin capping protein alpha during blood infection of the malaria parasite, Mol. Microbiol. 96 (2015) 84–94. https://doi.org/10.1111/mmi.12922.

[12]   M.B. Heintzelman, Cellular and Molecular Mechanics of Gliding Locomotion in Eukaryotes, Int. Rev. Cytol. 251 (2006) 79–129. https://doi.org/10.1016/S0074-7696(06)51003-4.

[13]   S. Münter, B. Sabass, C. Selhuber-Unkel, M. Kudryashev, S. Hegge, U. Engel, J.P. Spatz, K. Matuschewski, U.S. Schwarz, F. Frischknecht, Plasmodium Sporozoite Motility Is Modulated by the Turnover of Discrete Adhesion Sites, Cell Host Microbe. 6 (2009) 551–562. https://doi.org/10.1016/j.chom.2009.11.007.

[14]   J.P. VANDERBERG, Studies on the Motility of Plasmodium Sporozoites, J. Protozool. 21 (1974) 527–537. https://doi.org/10.1111/j.1550-7408.1974.tb03693.x.

[15]   S. Schmitz, M. Grainger, S. Howell, L.J. Calder, M. Gaeb, J.C. Pinder, A.A. Holder, C. Veigel, Malaria parasite actin filaments are very short, J. Mol. Biol. 349 (2005) 113–125. https://doi.org/10.1016/j.jmb.2005.03.056.

[16]   K.M. Skillman, C.I. Ma, D.H. Fremont, K. Diraviyam, J.A. Cooper, D. Sept, L.D. Sibley, The unusual dynamics of parasite actin result from isodesmic polymerization, Nat. Commun. 4 (2013). https://doi.org/10.1038/ncomms3285.

[17]   J. Vahokoski, S.P. Bhargav, A. Desfosses, M. Andreadaki, E.P. Kumpula, S.M.

Martinez, A. Ignatev, S. Lepper, F. Frischknecht, I. Sidén-Kiamos, C. Sachse, I. Kursula, Structural Differences Explain Diverse Functions of Plasmodium Actins, PLoS Pathog. 10 (2014). https://doi.org/10.1371/journal.ppat.1004091.

[18] E.P. Kumpula, I. Pires, D. Lasiwa, H. Piirainen, U. Bergmann, J. Vahokoski, I. Kursula, Apicomplexan actin polymerization depends on nucleation, Sci. Rep. 7 (2017) 1–10. https://doi.org/10.1038/s41598-017-11330-w.

[19] E.P. Kumpula, A.J. Lopez, L. Tajedin, H. Han, I. Kursula, Atomic view into plasmodium actin polymerization, ATP hydrolysis, and fragmentation, PLoS Biol. 17 (2019). https://doi.org/10.1371/journal.pbio.3000315.

[20] H. Lu, P.M. Fagnant, K.M. Trybus, Unusual dynamics of the divergent malaria parasite PfAct1 actin filament, Proc. Natl. Acad. Sci. U. S. A. 116 (2019) 20418–20427. https://doi.org/10.1073/pnas.1906600116.

[21] S. Pospich, E.P. Kumpula, J. Von Der Ecken, J. Vahokoski, I. Kursula, S. Raunser, Near-atomic structure of jasplakinolide-stabilized malaria parasite F-actin reveals the structural basis of filament instability, Proc. Natl. Acad. Sci. U. S. A. 114 (2017) 10636–10641. https://doi.org/10.1073/pnas.1707506114.

[22] J.M. Sattler, M. Ganter, M. Hliscs, K. Matuschewski, H. Schüler, Actin regulation in the malaria parasite, Eur. J. Cell Biol. 90 (2011) 966–971. https://doi.org/10.1016/j.ejcb.2010.11.011.

[23] E.P. Kumpula, I. Kursula, Towards a molecular understanding of the apicomplexan actin motor: On a road to novel targets for malaria remedies?, Acta Crystallogr. Sect. FStructural Biol. Commun. 71 (2015) 500–513. https://doi.org/10.1107/S2053230X1500391X.

[24] K. Matuschewski, J. Ross, S.M. Brown, K. Kaiser, V. Nussenzweig, S.H.I. Kappe, Infectivity-associated changes in the transcriptional repertoire of the malaria parasite sporozoite stage, J. Biol. Chem. 277 (2002) 41948–41953. https://doi.org/10.1074/jbc.M207315200.

[25] A. Ignatev, S.P. Bhargav, J. Vahokoski, P. Kursula, I. Kursula, The lasso segment is required for functional dimerization of the Plasmodium formin 1 FH2 domain, PLoS One. 7 (2012). https://doi.org/10.1371/journal.pone.0033586.

[26] A. Micsonai, F. Wien, L. Kernya, Y.H. Lee, Y. Goto, M. Réfrégiers, J. Kardos, Accurate secondary structure prediction and fold recognition for circular dichroism spectroscopy, Proc. Natl. Acad. Sci. U. S. A. 112 (2015) E3095–E3103. https://doi.org/10.1073/pnas.1500851112.

[27] S. Förster, L. Apostol, W. Bras, Scatter: Software for the analysis of nano-and mesoscale small-angle scattering, J. Appl. Crystallogr. 43 (2010) 639–646. https://doi.org/10.1107/S0021889810008289.

[28] D. Franke, M. V. Petoukhov, P. V. Konarev, A. Panjkovich, A. Tuukkanen, H.D.T. Mertens, A.G. Kikhney, N.R. Hajizadeh, J.M. Franklin, C.M. Jeffries, D.I. Svergun, ATSAS 2.8: A comprehensive data analysis suite for small-angle scattering from macromolecular solutions, J. Appl. Crystallogr. 50 (2017) 1212–1225. https://doi.org/10.1107/S1600576717007786.

[29] D.I. Svergun, Restoring low resolution structure of biological macromolecules from solution scattering using simulated annealing, Biophys. J. 76 (1999) 2879–2886. https://doi.org/10.1016/S0006-3495(99)77443-6.

[30] D. Franke, D.I. Svergun, DAMMIF, a program for rapid ab-initio shape determination in small-angle scattering, J. Appl. Crystallogr. 42 (2009) 342–346. https://doi.org/10.1107/S0021889809000338.

[31] A. Waterhouse, M. Bertoni, S. Bienert, G. Studer, G. Tauriello, R. Gumienny, F.T. Heer, T.A.P. De Beer, C. Rempfer, L. Bordoli, R. Lepore, T. Schwede, SWISS-MODEL: Homology modelling of protein structures and complexes, Nucleic Acids Res. 46 (2018) W296–W303. https://doi.org/10.1093/nar/gky427.

[32] A. Panjkovich, D.I. Svergun, SASpy: A PyMOL plugin for manipulation and refinement of hybrid models against small angle X-ray scattering data, Bioinformatics. 32 (2016) 2062–2064. https://doi.org/10.1093/bioinformatics/btw071.

[33] L. Schrödinger, The PyMOL Molecular Graphics System, Version 2.0, (2015).

[34] E.P. Kumpula, I. Pires, D. Lasiwa, H. Piirainen, U. Bergmann, J. Vahokoski, I. Kursula, Apicomplexan actin polymerization depends on nucleation, Sci. Rep. 7

(2017). https://doi.org/10.1038/s41598-017-11330-w.

[35] K. Remmert, D. Vullhorst, H. Hinssen, In vitro refolding of heterodimeric CapZ expressed in E. coli as inclusion body protein, Protein Expr. Purif. 18 (2000) 11–19. https://doi.org/10.1006/prep.1999.1132.

[36] Y. Soeno, H. Abe, S. Kimura, K. Maruyama, T. Obinata, Generation of functional β-actinin (CapZ) in an E. coli expression system, J. Muscle Res. Cell Motil. 19 (1998) 639–646. https://doi.org/10.1023/A:1005329114263.

[37] M.A. Wear, A. Yamashita, K. Kim, Y. Maéda, J.A. Cooper, How capping protein binds the barbed end of the actin filament, Curr. Biol. 13 (2003) 1531–1537. https://doi.org/10.1016/S0960-9822(03)00559-1.

[38] A. Narita, S. Takeda, A. Yamashita, Y. Maéda, Structural basis of actin filament capping at the barbed-end: A cryo-electron microscopy study, EMBO J. 25 (2006) 5626–5633. https://doi.org/10.1038/sj.emboj.7601395.

[39] T. Kim, J.A. Cooper, D. Sept, The Interaction of Capping Protein with the Barbed End of the Actin Filament, J. Mol. Biol. 404 (2010) 794–802. https://doi.org/10.1016/j.jmb.2010.10.017.

[40] I. Kursula, P. Kursula, M. Ganter, S. Panjikar, K. Matuschewski, H. Schüler, Structural Basis for Parasite-Specific Functions of the Divergent Profilin of Plasmodium falciparum, Structure. 16 (2008) 1638–1648. https://doi.org/10.1016/j.str.2008.09.008.

[41] C.A. Moreau, S.P. Bhargav, H. Kumar, K.A. Quadt, H. Piirainen, L. Strauss, J. Kehrer, M. Streichfuss, J.P. Spatz, R.C. Wade, I. Kursula, F. Frischknecht, A unique profilin-actin interface is important for malaria parasite motility, PLoS Pathog. 13 (2017) e1006412. https://doi.org/10.1371/journal.ppat.1006412.

[42] E. Deligianni, R.N. Morgan, L. Bertuccini, T.W.A. Kooij, A. Laforge, C. Nahar, N. Poulakakis, H. Schüler, C. Louis, K. Matuschewski, I. Siden-Kiamos, Critical role for a stage-specific actin in male exflagellation of the malaria parasite, Cell. Microbiol. 13 (2011) 1714–1730. https://doi.org/10.1111/j.1462-5822.2011.01652.x.

[43] J.G. Wesseling, P.J.F. Snijders, P. van Someren, J. Jansen, M.A. Smits, J.G.G. Schoenmakers, Stage-specific expression and genomic organization of the actin genes of the malaria parasite Plasmodium falciparum, Mol. Biochem. Parasitol. 35 (1989) 167–176. https://doi.org/10.1016/0166-6851(89)90119-9.

[44] E.A. Barron-Casella, M.A. Torres, S.W. Scherer, H.H.Q. Heng, L.C. Tsui, J.F. Casella, Sequence analysis and chromosomal localization of human Cap Z: Conserved residues within the actin-binding domain may link Cap Z to gelsolin/severin and profilin protein families, J. Biol. Chem. 270 (1995) 21472–21479. https://doi.org/10.1074/jbc.270.37.21472.

[45] M.C. Hart, Y.O. Korshunova, J.A. Cooper, Vertebrates have conserved capping protein α isoforms with specific expression patterns, Cell Motil. Cytoskeleton. 38 (1997) 120–132. https://doi.org/10.1002/(SICI)1097-0169(1997)38:2<120::AID-CM2>3.0.CO;2-B.

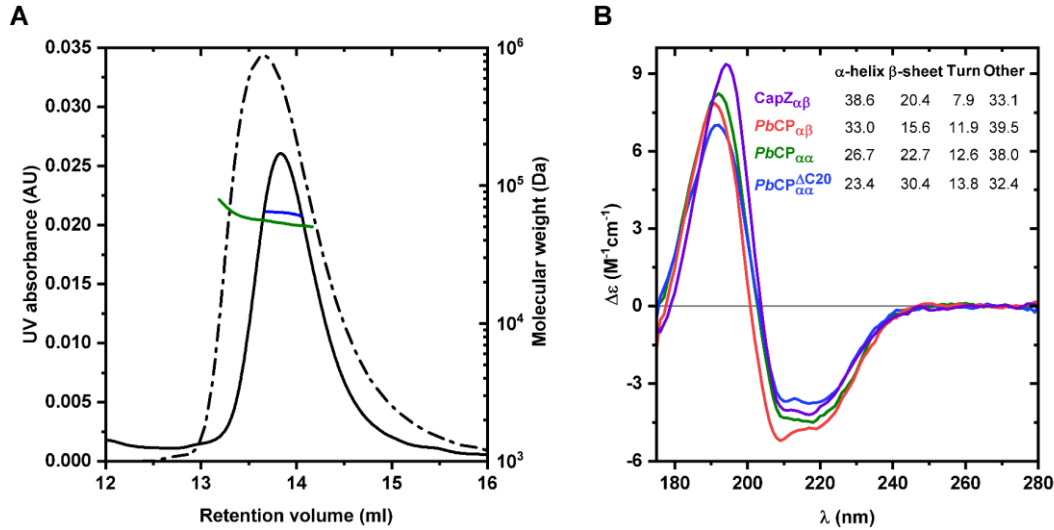[46] M.C. Hart, J.A. Cooper, Vertebrate isoforms of actin capping protein β have distinct functions in vivo, J. Cell Biol. 147 (1999) 1287–1298. https://doi.org/10.1083/jcb.147.6.1287.

Figure 1. *Pb*CPα forms folded homodimers in solution. **(A)** SLS of *Pb*CPαα and *Pb*CPαα$^{\Delta C20}$. The UV signal is denoted by a black dotted or solid line and the SLS signal in green or blue for the full-length and truncated *Pb*CPαα, respectively. AU = arbitrary unit. The calculated molecular weight is 66.44±0.13 kDa for *Pb*CPαα and 63.55±0.13 kDa for *Pb*CPαα$^{\Delta C20}$. **(B)** SRCD spectra of CapZαβ (purple), *Pb*CPαβ (red), *Pb*CPαα (green), and *Pb*CPαα$^{\Delta C20}$ (blue). The table in the inset shows the major secondary structure components of the different CPs, as deconvolved using BeStSel.
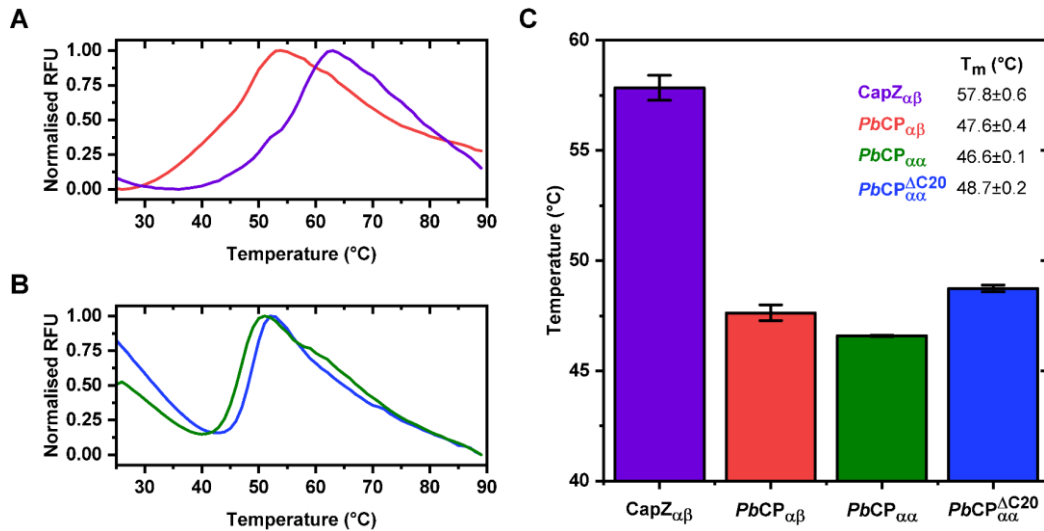
Figure 2. Thermal unfolding of CPs. **(A)** Normalized raw denaturation signals of the heterodimer CapZαβ (purple) and *Pb*CPαβ (red). RFU = relative fluorescence unit. **(B)** Normalized raw denaturation signals of the homodimer *Pb*CPαα (green) and *Pb*CPαα$^{\Delta C20}$ (blue). **(C)** Calculated melting temperatures (T_m) of the different CPs. The temperatures were derived from fitted Boltzmann equations. Error bars represent SD (n=3).
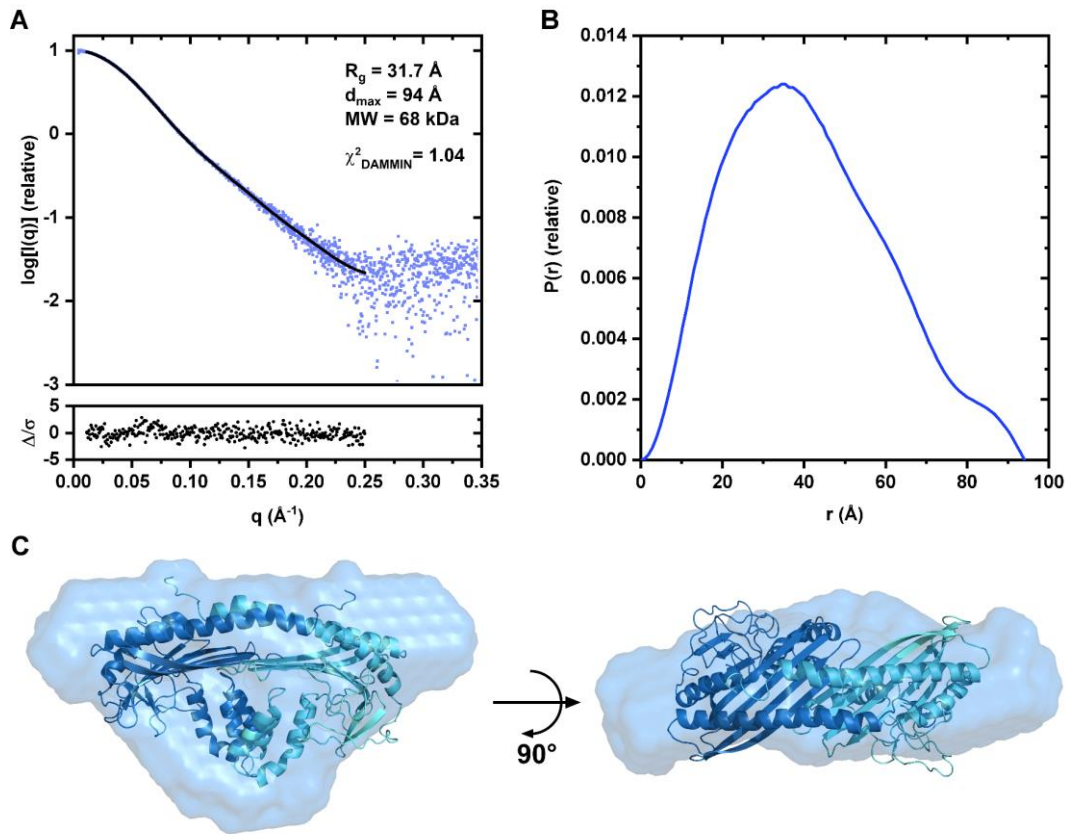
Figure 3. Solution structure of the *Pb*CPαα$^{\Delta C20}$ homodimer. **(A)** Fit of a DAMMIN *ab initio* model (black line) to the experimental scattering curve on a relative scale (light blue dots) with ScÅtter-calculated parameters and fit including the χ^2 value in the inset. The lower graph denotes weighted residual errors of the fit (black dots), where $\Delta/\sigma = [I_{exp}(q) - c \cdot I_{mod}(q)]/\sigma(q)$. **(B)** Real-space distance distribution plot. **(C)** DAMMIN bead model (light blue envelope) superimposed with the *Pb*CPαα$^{\Delta C20}$ homology model (cartoon).
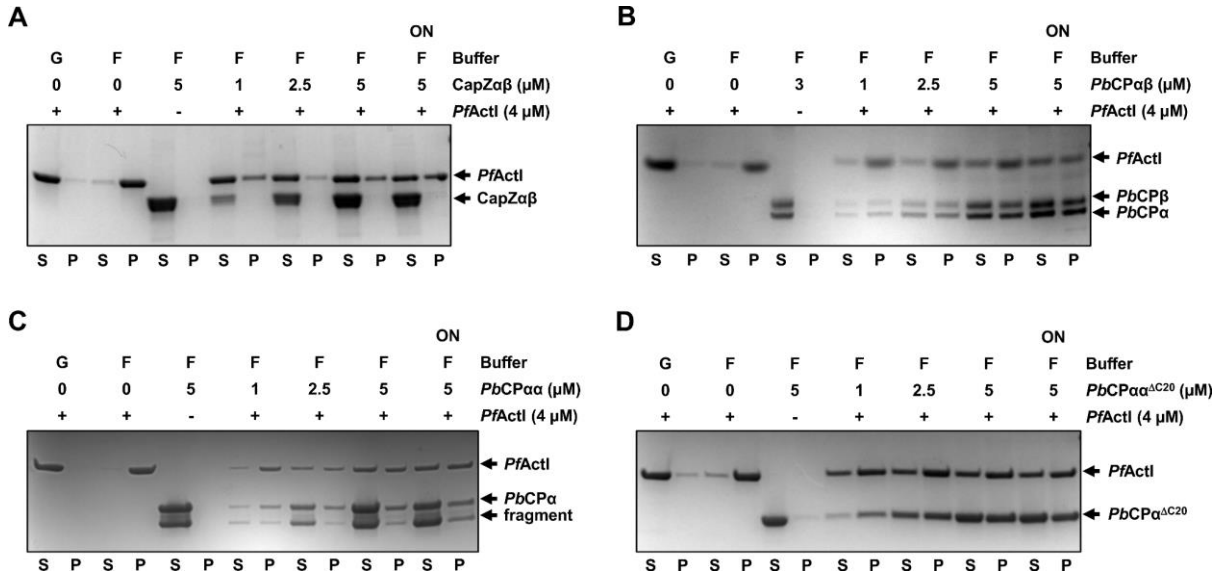
Figure 4. *Pb*CPs bind *Pf*ActI filaments. **(A)** CapZαβ. **(B)** *Pb*CPαβ. **(C)** *Pb*CPαα. **(D)** *Pb*CPαα$^{\Delta C20}$. G: G-buffer; F: F-buffer; S: supernatant; P: pellet; ON: pre-incubation of the CPs with *Pf*ActI for 8-16 h. The images have been slightly histogram adjusted for clarity.

Functional homo- and heterodimeric actin capping proteins from the malaria parasite

Ábris Ádám Bendes, Moon Chatterjee, Benjamin Götte, Petri Kursula, Inari Kursula

SUPPLEMENTARY METHODS

Label-free unfolding analysis

Unfolding of the *Plasmodium* CPs was measured in SEC buffer on a Prometheus NT.48 instrument (NanoTemper Technologies, DE) at concentrations between 1.8 and 9.0 mg/ml using a temperature range 20-95°C at 1°C/min ramping speed. The data were analyzed using the PR.ThermControl software (NanoTemper Technologies, DE). We are grateful to Dr. Jakub Nowak for help with the Prometheus NT.48 instrument.

Mass spectroscopy (MS)

Molecular weights of the *Pb*CPαα degradation products were determined using a Synapt G1 ESI-LCMS Q-TOF instrument (Waters, GB) connected to an Acquity UPLC system (Waters, GB). *Pb*CPαα was incubated on ice for a week before processing. The protein sample was diluted in 0.1% trifluoroacetic acid and eluted on a BEH C_4 300 column (Waters, GB) using a 60% acetonitrile gradient in 0.1% formic acid mobile phase. Mass spectra were deconvolved using the MassLynx software with the MaxEnt 1 algorithm (Waters, GB).
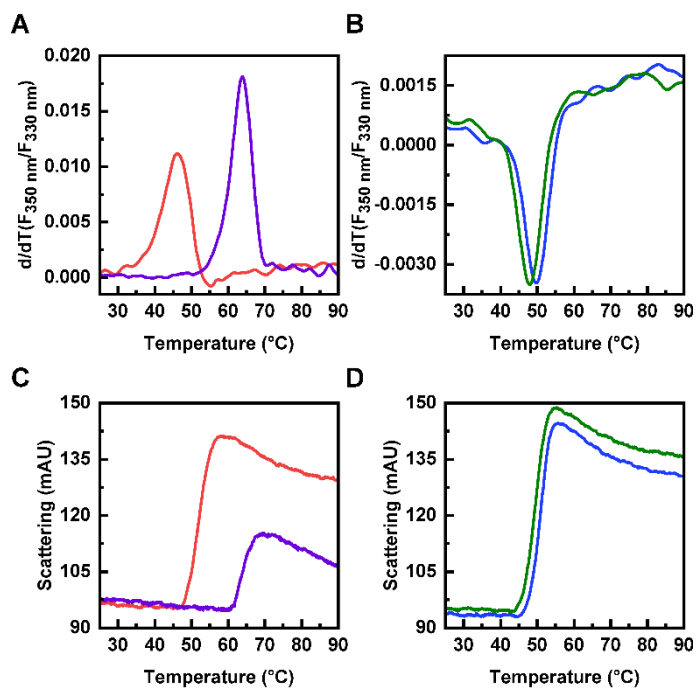
SUPPLEMENTARY FIGURES

Figure S1. Thermal denaturation of CPs. **(A)** First derivative of the ratio of the fluorescence signals during unfolding of CapZαβ (purple) and *Pb*CPαβ (red). **(B)** Denaturation signal of *Pb*CPαα (green) and *Pb*CPαα$^{\Delta C20}$ (blue). **(C)** Aggregation levels during thermal ramping of CapZαβ (purple) and *Pb*CPαβ (red). AU = arbitrary unit. **(D)** Aggregation of *Pb*CPαα (green) and *Pb*CPαα$^{\Delta C20}$ (blue).

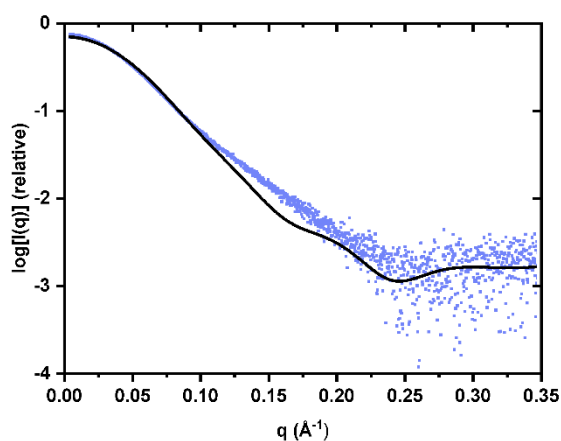**Figure S2.** CRYSOL [1] calculated fit of the *Pb*CPαα$^{\Delta C20}$ homology model (black line) to the experimental SAXS data (light blue dots).

A

B

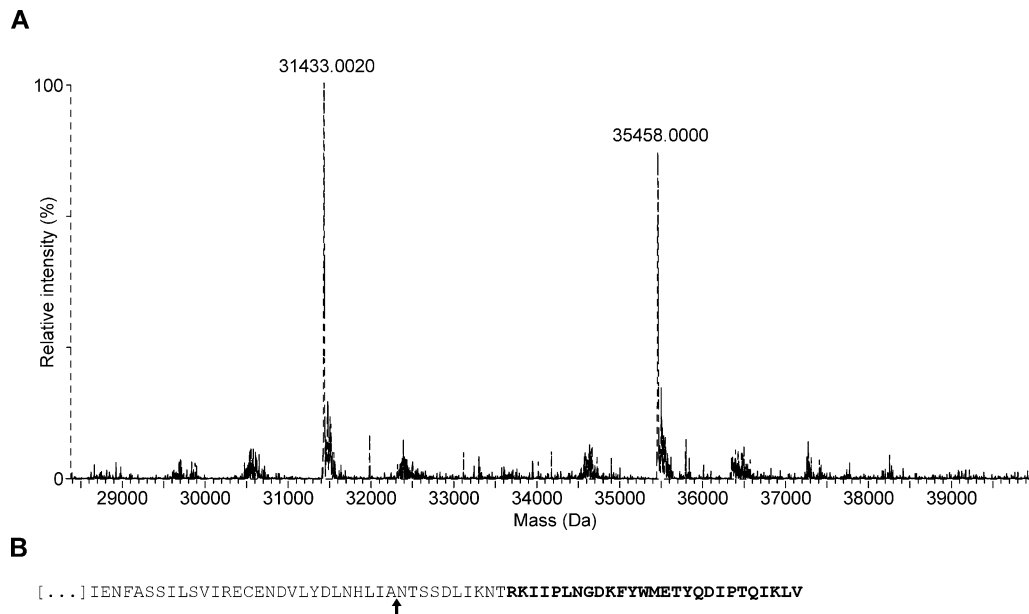[...]IENFASSILSVIRECENDVLYDLNHLIANTSSDLIKNT**RKIIPLNGDKFYWMETYQDIPTQIKLV**

Figure S3. Mass spectroscopy of *Pb*CPαα fragments. **(A)** Intensity distribution of the two governing *Pb*CPαα species. **(B)** Well defined cleavage point on the C-terminus of *Pb*CPα. Bold text denotes the α-tentacle region.

SUPPLEMENTARY REFERENCE

[1]   D. Svergun, C. Barberato, M.H. Koch, CRYSOL - A program to evaluate X-ray solution scattering of biological macromolecules from atomic coordinates, J. Appl. Crystallogr. 28 (1995) 768–773. https://doi.org/10.1107/S0021889895007047.